diagnostics

MDPI

Review

Anatomical Validity of MRI-Based Choroid Plexus Segmentation: Regional Boundaries, Age-Related Morphology, and Implications for Neuroimaging Biomarkers

Michele Cerasuolo [1,2,*], Francesco Spada [3], Umberto Galdiero [4], Nicholas Giulio Raccagni [5], Simone Laguardia [5] and Gary Antonio Barahona Rodriguez [6]

[1] Division of Human Anatomy, Neuronal Networks Morphology & Systems Biology Lab, Department of Mental and Physical Health and Preventive Medicine, University of Campania "Luigi Vanvitelli", 80138 Naples, Italy
[2] Neuromodulation Center and Center for Clinical Research Learning, Spaulding Rehabilitation Hospital, Harvard Medical School, 1575 Cambridge Street, Cambridge, MA 02138, USA
[3] Beaumont Hospital, Beaumont Road, D09 V2N0 Dublin, Ireland; francescospada@beaumont.ie
[4] ISGlobal, Hospital Clínic, Universitat de Barcelona, 08036 Barcelona, Spain; umbertogald@gmail.com
[5] School of Medicine and Surgery, University of Milano-Bicocca, 20126 Milan, Italy; n.raccagni@campus.unimib.it (N.G.R.); s.laguardia@campus.unimib.it (S.L.)
[6] Beth Israel Deaconess Medical Center, Harvard Medical School, Boston, MA 02115, USA; gbaraho1@bidmc.harvard.edu
* Correspondence: michele.cerasuolo@unicampania.it; Tel.: +39-3911116754

Abstract

Magnetic resonance imaging (MRI)-derived choroid plexus (ChP) volume is increasingly investigated in studies of brain aging and neurodegeneration, yet its anatomical meaning remains uncertain because segmentation methods differ in ventricular coverage, image contrast, and reference annotations. This narrative review examines the anatomical basis and methodological validity of ChP volumetry by integrating evidence on ventricular anatomy, age-related tissue changes, manual and automated segmentation, and associations with cognitive impairment and Alzheimer's disease. The lateral ventricular ChP, particularly the atrial glomus, is generally easier to delineate on conventional MRI than its thin extensions and the third and fourth ventricular components. Segmentation performance depends on the anatomical reference and acquisition protocol; agreement with manually drawn masks does not necessarily establish complete anatomical coverage. In addition, age-related vascular remodeling, changes in stromal composition, calcification, and cystic alterations can affect MRI appearance and the interpretation of total volume. Although ChP enlargement has been associated with aging, cognitive impairment, and Alzheimer's disease, volume alone cannot identify the contributing tissue compartments or establish blood–cerebrospinal fluid barrier dysfunction. We propose an anatomy-centered approach to ChP volumetry based on explicit regional definitions, complementary measures of spatial and volumetric accuracy, assessment of test–retest and multicenter reliability, and independent biological validation when functional interpretations are intended.

Keywords: choroid plexus; magnetic resonance imaging; anatomical validity; image segmentation; volumetry; brain aging; Alzheimer's disease; neuroimaging biomarkers; blood–cerebrospinal fluid barrier

Check for updates

Academic Editor: Ji-Hyun Lee

Received: 25 October 2026
Revised: 3 November 2026
Accepted: 10 November 2026
Published: 11 November 2026

Copyright: © 2026 by the authors. Licensee MDPI, Basel, Switzerland. This article is an open access article distributed under the terms and conditions of the Creative Commons Attribution (CC BY) license.

1. Introduction

The choroid plexus (ChP) is a highly vascularized epithelial structure located within the lateral, third, and fourth cerebral ventricles, where it contributes to cerebrospinal fluid

(CSF) secretion and constitutes the anatomical basis of the blood–CSF barrier [1,2]. Its organization consists of a vascularized connective tissue core covered by a specialized epithelial monolayer, with regional differences in morphology, spatial arrangement, and relationships with adjacent ventricular structures. Within the lateral ventricles, the ChP extends along the choroidal fissure and is particularly prominent in the atrium, whereas its smaller components in the third and fourth ventricles present distinct anatomical boundaries that are more difficult to delineate using conventional structural magnetic resonance imaging (MRI) [1]. These characteristics complicate the translation of gross anatomical definitions into reproducible volumetric measurements, particularly when imaging protocols do not provide sufficient contrast or spatial resolution to separate the ChP from surrounding CSF and neural tissue [1,3].

Interest in MRI-derived ChP measurements has increased following reports of volumetric alterations associated with aging, cognitive impairment, and neurodegenerative diseases [3–6]. A systematic review and meta-analysis published in 2026, including 16 studies, identified greater ChP volume in patients with Alzheimer's disease (AD) than in healthy controls, although the included studies differed in imaging and segmentation methods [5]. In a longitudinal investigation involving 564 participants without dementia, the longitudinal analysis identified associations between ChP morphological characteristics, amyloid and tau pathology, and subsequent cognitive decline, suggesting that structural features beyond total volume may be clinically informative [4]. More recently, a UK Biobank study involving 45,306 participants reported associations of greater MRI-derived ChP volume and lower signal intensity with cognitive impairment and incident dementia [6]. Although these findings support further investigation of ChP morphology as a potential imaging biomarker, their interpretation depends on the anatomical structures captured by the segmentation procedures and the extent to which measurement differences reflect tissue changes rather than imaging-related variability [3,6,7].

The literature was identified through targeted searches of PubMed/MEDLINE, Scopus, and Web of Science, complemented by examination of reference lists from relevant original articles and reviews. Search terms included combinations of "choroid plexus", "MRI", "magnetic resonance imaging", "segmentation", "volumetry", "neuroanatomy", "aging", "Alzheimer's disease", and "neurodegeneration". Studies were considered according to their relevance to four predefined areas: (i) gross and microscopic ChP anatomy; (ii) age-related morphological and microstructural changes; (iii) manual and automated MRI segmentation methods, including anatomical reference standards and validation metrics; and (iv) clinical associations with cognitive impairment and neurodegenerative disorders. Publications were assessed for relevance based on their titles, abstracts, and full texts when necessary. Particular attention was given to original investigations providing quantitative morphometric data, explicit segmentation procedures, or methodological validation, while foundational anatomical studies and relevant reviews were included for contextual interpretation. Given the narrative design, no formal meta-analysis or exhaustive systematic screening was undertaken. Previous systematic reviews have summarized ChP volume alterations across brain disorders [8] and Alzheimer's disease [5], while acknowledging methodological heterogeneity in segmentation approaches. However, these syntheses have primarily addressed clinical associations rather than systematically examining how MRI-defined segmentation boundaries correspond to the anatomical extent of the ChP across ventricular compartments. This distinction remains unresolved, particularly regarding regional coverage, reference annotations, and age-related tissue changes that may affect volumetric interpretation. The present review addresses this gap by distinguishing three related but conceptually different dimensions of ChP volumetry. Segmentation accuracy refers to the agreement between an automated segmentation and a predefined imaging reference, typically assessed through

spatial overlap, boundary distances, and volumetric error. Anatomical validity concerns whether the segmented region accurately represents the intended ChP structures and ventricular compartments, including their boundaries and regional extent. Biological validity refers to the extent to which MRI-derived measurements correspond to the underlying tissue characteristics or physiological processes they are intended to represent. Importantly, high segmentation accuracy does not necessarily establish anatomical validity, and neither property independently demonstrates biological validity.

Based on this synthesis, we propose an anatomy-centered framework for defining segmentation targets and evaluating the validity of ChP-derived neuroimaging biomarkers.

Figure 1 illustrates the anatomical and methodological considerations underlying ChP volumetry, highlighting the regional distribution and MRI-visible boundaries of the ChP within the lateral, third, and fourth ventricles. The figure also summarizes the principal anatomical factors influencing segmentation and presents the proposed validation framework, distinguishing segmentation accuracy, anatomical validity, and biological validity. The illustrated boundaries are schematic and should not be interpreted as independently validated segmentation masks.

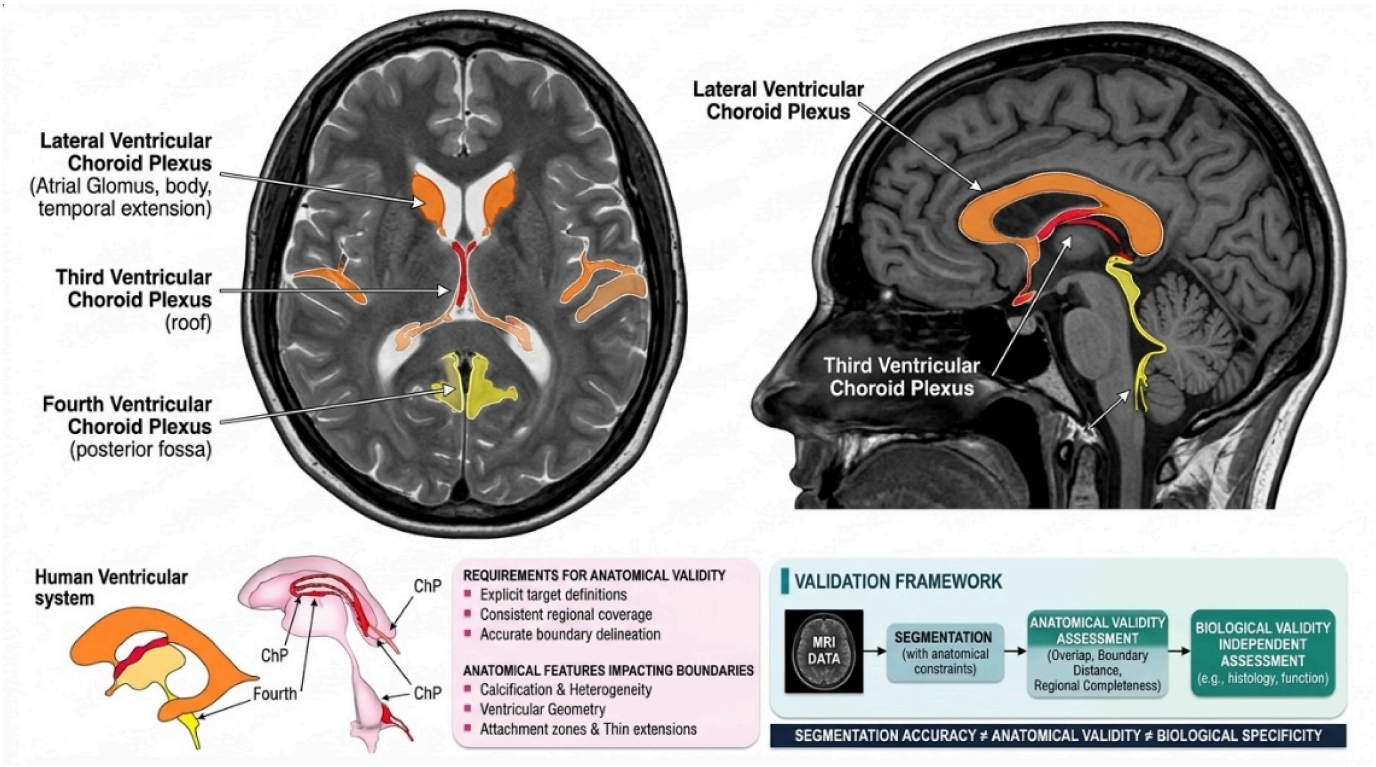


Figure 1. Anatomical and methodological considerations for interpreting MRI-derived choroid plexus volumetry. Anatomical illustrations showing the regional distribution and boundaries of the choroid plexus (ChP) within the ventricular system. The upper axial and sagittal MRI-based illustrations schematically highlight the lateral ventricular ChP (orange), including its atrial and temporal extensions, the third ventricular ChP (red), and the fourth ventricular ChP (yellow). These representations illustrate the anatomical relationships relevant to MRI-based segmentation and the challenges associated with delineating smaller ventricular components. The colored regions are schematic and do not represent independently validated segmentation masks or histologically confirmed boundaries. The lower-left illustrations depict the ventricular anatomy of the ChP and summarize factors influencing anatomical delineation, including regional heterogeneity, calcification, ventricular geometry, and attachment zones. The lower-right schematic presents the proposed validation framework, distinguishing segmentation accuracy, anatomical validity, and biological validity as complementary

dimensions of MRI-derived ChP volumetry. Together, these elements illustrate the need for explicit anatomical definitions, reproducible segmentation procedures, and independent biological validation before interpreting ChP volume as a neuroimaging biomarker. Image sources, copyright information, and AI-assisted illustration: The anatomical illustration of the ventricular system was adapted (cropped and resized) from [9]. Licensed under the Creative Commons Attribution 4.0 International License (CC BY 4.0, https://creativecommons.org/licenses/by/4.0/). Google Gemini (free web-based version, Auto mode; Google LLC) was used to assist in generating selected illustrative elements of the figure. The anatomical annotations, conceptual framework, and final figure composition were prepared by the authors.

2. Anatomical Organization of the Choroid Plexus

2.1. Gross Anatomy and Ventricular Distribution

The choroid plexus (ChP) forms a series of highly vascularized, folded structures within the lateral, third, and fourth ventricles. Although these structures share a common epithelial–stromal organization, their macroscopic configuration, anatomical attachments, and relationships with surrounding neural tissue differ substantially across ventricular compartments [10,11]. These regional characteristics are particularly relevant to neuroimaging because the anatomical extent of the ChP cannot be defined using a single set of ventricular landmarks. Within each lateral ventricle, the ChP extends along the choroidal fissure, a C-shaped cleft situated between the fornix and the thalamus. The fissure extends from the region of the interventricular foramen of Monro through the ventricular body and atrium into the inferior horn, where it follows the medial ventricular boundary toward the inferior choroidal point [11]. The lateral ventricular ChP is therefore distributed predominantly within the body, atrium, and temporal horn, rather than throughout the entire ventricular cavity. Its most conspicuous enlargement, traditionally described as the glomus choroideum, is located in the atrium, where the folded vascular tissue forms an irregular and relatively bulky structure that is readily identifiable on many conventional MRI acquisitions [2,11].

The anatomical relationship between the ChP and adjacent structures changes along this trajectory. In the ventricular body, the ChP lies close to the thalamus and fornix, whereas its temporal extension follows the medial aspect of the inferior horn in proximity to the hippocampal formation. These relationships provide useful anatomical landmarks but also create potential difficulties in distinguishing the ChP from adjacent ventricular walls and neural structures, particularly when tissue contrast is limited [1,11]. The highly folded surface of the glomus and the progressive narrowing of the temporal extension further contribute to regional differences in the visibility of ChP boundaries on MRI. The ChP of the third ventricle occupies the superior portion of the ventricular cavity and is associated with the tela choroidea forming part of its roof. Its location places it in close anatomical relationship with the fornix, thalamic structures, and internal cerebral veins, which must be distinguished from ChP tissue during image interpretation [1,10]. Compared with the lateral ventricular glomus, the third ventricular ChP is smaller and generally less conspicuous on routine structural MRI, making its identification more dependent on spatial resolution and multiplanar anatomical assessment.

The fourth ventricular ChP presents a different configuration, arising from the tela choroidea associated with the inferior portion of the ventricular roof. Its architecture includes medial and lateral portions extending toward the median and lateral apertures of the fourth ventricle [12,13]. The lateral extensions may protrude through the foramina of Luschka into the cerebellopontine cisterns, forming the structures traditionally known as Bochdalek's flower baskets. Cadaveric morphometric investigations have demonstrated considerable variability in their dimensions, exposure, and relationships with adjacent neurovascular structures [14]. This arrangement is important for anatomical delineation

because portions of the fourth ventricular ChP may extend beyond the apparent ventricular cavity and lie adjacent to cerebellar, brainstem, and subarachnoid structures [12,14].

2.2. Microscopic Organization and the Blood–CSF Barrier

At the microscopic level, the ChP is composed of a monolayer of specialized epithelial cells surrounding a vascularized connective tissue stroma. The epithelial cells are generally cuboidal and exhibit apical microvilli, basolateral membrane infoldings, and abundant mitochondria, consistent with their polarized secretory and transport functions. The epithelium rests on a basement membrane and is continuous with the ventricular lining at the attachment of the ChP, although its junctional organization and permeability properties differ from those of the surrounding ependyma [10]. The vascular compartment consists of an extensive network of predominantly fenestrated capillaries embedded within connective tissue containing extracellular matrix components, fibroblasts, and immune cells. Unlike the largely nonfenestrated capillary endothelium of the blood–brain barrier, ChP capillaries permit relatively extensive exchange between blood and stroma, while epithelial tight junctions constitute the principal anatomical barrier regulating paracellular movement toward the CSF. The resulting blood–CSF barrier is therefore organized primarily at the epithelial level rather than through the endothelial barrier architecture characteristic of [15] most cerebral microvessels [16].

The ChP stroma contains several additional cellular populations, including resident macrophages, dendritic cells, and other immune cells. Epiplexus macrophages, commonly referred to as Kolmer cells, are located on the CSF-facing surface of the epithelium and represent a cellular compartment distinct from the underlying vascular and stromal components. Consequently, ChP tissue is not a homogeneous epithelial structure but a composite anatomical compartment containing epithelial, vascular, connective tissue, and immune elements [17]. At the epithelial interface, inflammatory signals may also regulate trafficking of peripheral immune cells into the CNS.

2.3. Regional Cellular Heterogeneity

Beyond macroscopic differences, experimental evidence indicates that ChP cellular organization and molecular characteristics vary according to ventricular location. In a single-cell and spatial transcriptomic investigation of developing, adult, and aged mice, single-cell and spatial transcriptomic analyses identified heterogeneous epithelial, endothelial, mesenchymal, and immune populations across the lateral, third, and fourth ventricular ChP. Epithelial cells and fibroblasts exhibited ventricle-associated transcriptional profiles, with regional differences emerging during development and persisting into adulthood [17]. These regional molecular findings derive from mice and cannot be directly translated into human MRI-defined boundaries. Differences in cellular phenotype occur at spatial scales far smaller than those resolved by routine structural imaging.

3. Aging and Choroid Plexus Morphology

3.1. Epithelial and Stromal Remodeling

The relationship between epithelial morphology and aging is not entirely consistent across experimental and human investigations. Earlier histological observations described reductions in epithelial cell height with aging across several species. However, a human postmortem investigation examined ChP epithelial morphology in 20 individuals aged 59–92 years, including patients with Alzheimer's disease (AD), vascular dementia, Parkinson's disease, multiple system atrophy, and controls. The investigators observed positive associations between age and epithelial cell area and dimensions, without significant differences in these measurements among diagnostic groups. These findings suggest that

age-related epithelial remodeling cannot be adequately characterized by a single directional change in cell size [18].

3.2. Age-Related Volume Changes

Several human MRI studies have identified positive associations between age and ChP volume. In 155 cognitively unimpaired adults aged 21–94 years, MRI measurements showed an age-related increase in ChP volume, accompanied by enlargement of the lateral ventricles. Both measurements exhibited nonlinear relationships with age after normalization to intracranial volume, suggesting that ChP enlargement occurs alongside broader changes in ventricular anatomy [19]. An independent analysis evaluated age-related ChP volumetry using deep learning models applied to T1-weighted, T2-weighted, and FLAIR images. In 98 adults aged 21–89 years, ChP volume increased significantly with age across all three MRI sequences (all $p < 0.001$), with coefficients of determination ranging from 0.54 to 0.60. The consistency of these findings across imaging sequences supports the presence of an age-associated volumetric pattern, although the measurements remain dependent on the anatomical definitions and reference segmentations used to develop the models [3].

In 641 healthy adults aged 36–90 years from the Human Connectome Project–Aging dataset, imaging showed an increase in ChP volume with age ($r^2 = 0.20$, $p < 0.001$). A subsequent population-based study examined 45,306 participants from the UK Biobank and reported a positive correlation between age and MRI-derived ChP volume ($r = 0.49$, $p < 0.001$), together with a negative correlation between age and ChP signal intensity ($r = -0.44$, $p < 0.001$) [6]. These findings extend the observation of age-associated ChP enlargement to a large population-based cohort [20]. A separate lifespan analysis of 5551 participants provided reference trajectories for ChP volume and shape, including measurements normalized to brain and ventricular size [21]. Longitudinal evidence is more limited but provides additional information about within-person volumetric changes. A longitudinal investigation analyzed 2334 MRI observations from 613 participants in the Alzheimer's Disease Neuroimaging Initiative, including cognitively unimpaired individuals and participants with cognitive impairment. The analysis showed an overall increase in ChP volume of 14.92 mm^3 per year (95% CI, 11.05–18.77) [22], with differences according to sex, cognitive trajectory, and APOE ε4 genotype. Because this cohort included participants across different cognitive and diagnostic categories, these findings cannot be interpreted as a normative rate of ChP enlargement attributable exclusively to healthy aging.

An important contrast emerges from experimental research. Using two dedicated high-resolution MRI protocols, investigators examined the lateral ventricular ChP in young and aged mice and found significantly lower volumes in the older group. The study used 9.4-T MRI with 0.1–0.125 mm isotropic resolution and demonstrated relatively low test–retest variability for manual segmentation. These findings differ from the age-associated enlargement reported in human MRI cohorts, but differences in species, ventricular morphology, acquisition resolution, and segmentation procedures preclude direct interpretation of the results as contradictory measurements of the same biological phenomenon [7].

Pediatric populations provide a complementary perspective on ChP morphology, as several confounding factors associated with advanced aging, including neurodegenerative changes and calcification, are generally less prominent. An investigation involving 90 children aged 0–16 years established reference measurements of ChP thickness without identifying consistent age-related trends [23]. More recently, an automated MRI study involving 123 children with epilepsy and 108 healthy controls found no significant between-group differences in absolute or normalized ChP volume, hemispheric asymmetry, or ChP-to-ventricle volume ratios [24]. In contrast, a study of pediatric-onset multiple sclerosis identified greater normalized ChP volume compared with healthy controls using

manual segmentation, with ChP volume also associated with ventricular size [25]. These findings suggest that pediatric ChP morphology may differ according to clinical condition, while highlighting the need to distinguish developmental variation from disease-associated changes. Differences in anatomical coverage, segmentation methodology, and ventricular dimensions should therefore be considered when comparing ChP measurements across age groups.

3.3. Vascular and Microstructural Changes

Volumetric enlargement does not necessarily indicate preservation or expansion of the vascular compartment of the ChP. In 49 adults without neurological disorders, ferumoxytol-enhanced 7-T MRI was used to characterize ChP vascular architecture and distinguish vascular from nonvascular regions. Older participants exhibited lower vascular density than younger participants ($16.5 \pm 4.34\%$ versus $24.85 \pm 6.84\%$), together with a lower ferumoxytol-induced susceptibility change (22.10 ± 12.82 versus 34.64 ± 12.69 ppb). Vascular density was negatively correlated with age ($r = -0.48$), providing in vivo evidence of age-associated changes in the relative vascular component of the ChP [2]. Complementary observations were obtained using quantitative MRI in larger cohorts. An earlier quantitative MRI study identified lower ChP cerebral blood flow (CBF), increased longitudinal and transverse relaxation times, higher mean diffusivity, and lower fractional anisotropy with advancing age [19]. In the Human Connectome Project–Aging cohort, complementary measurements showed age-associated reductions in ChP perfusion ($r^2 = 0.17$, $p < 0.001$) and increases in mean diffusivity ($r^2 = 0.16$, $p < 0.001$) [20]. These findings indicate that age-related volumetric enlargement may coexist with changes in perfusion and MRI-derived microstructural characteristics. A 3-T MRI investigation of 77 adults similarly found that ChP volume increased with age while ChP perfusion decreased [26]. However, these MRI parameters are indirect measures of tissue properties. Diffusion and relaxation measurements are influenced by water distribution, tissue composition, and acquisition characteristics, while perfusion estimates depend on the assumptions underlying the imaging and quantification methods. Accordingly, the combination of increased ChP volume and reduced perfusion should not be interpreted as direct histological evidence of epithelial hypertrophy, stromal expansion, or vascular degeneration without appropriate validation.

3.4. Calcification and Cystic Alterations

Age-related changes in ChP morphology also include mineralized and cystic components, which may influence the interpretation of total-volume measurements. Calcifications are frequently identified within the ChP stroma and can be detected using computed tomography (CT), whereas their assessment using conventional MRI is more dependent on sequence characteristics and susceptibility effects. In 166 cognitively normal individuals, a multimodal imaging study examined MRI-derived ChP volume and CT-derived calcification volume in relation to age, APOE ε4 status, and hippocampal volume. ChP calcification volume was positively associated with overall ChP volume, but the two measurements exhibited different relationships with hippocampal volume. Calcification was not independently associated with lower hippocampal volume in the overall sample, while genotype-dependent associations were observed in analyses involving APOE ε4 carriers. These results suggest that calcification burden and overall ChP volume should not be treated as interchangeable morphological indicators [27].

A more recent study developed an automated segmentation framework for ChP calcifications using quantitative susceptibility mapping (QSM). In a validation subset of 22 participants, QSM-derived calcification volumes correlated with CT-derived measurements ($r = 0.728$). Application of the method to an additional cohort of 91 participants identified

increasing calcification volume and more diamagnetic susceptibility values with age. These findings demonstrate the feasibility of assessing a mineralized component separately from the overall ChP segmentation, although agreement with CT does not establish the biological significance of the detected deposits [28]. Cystic alterations represent another distinct morphological feature. A multisequence 7-T MRI study [29] investigated ChP cysts in healthy younger and older adults and patients with neurological disorders. The prevalence of cysts was higher in older than younger healthy controls, although this difference was only marginally significant. Patients with AD exhibited a higher cyst number and prevalence than the comparison groups, and cyst number and size were associated with overall ChP volume. These findings indicate that cystic components may contribute to apparent ChP enlargement, but their inclusion in volumetric measurements depends on the segmentation criteria and the MRI sequences used to identify them.

3.5. Implications for Volumetric Interpretation

The coexistence of ventricular enlargement, tissue-composition changes, and variable ChP morphology introduces several methodological considerations when interpreting age-related volumetric differences. As demonstrated by Alisch et al., both lateral ventricular and ChP volumes increase with age, highlighting the need to examine ChP measurements in relation to surrounding ventricular anatomy [19]. Although adjustment for intracranial volume accounts for differences in overall cranial size, it does not necessarily resolve the effects of ventricular enlargement on boundary identification or partial-volume contamination. Age-dependent vascular, cystic, and mineralized changes may also alter ChP image contrast. Whether these changes reduce segmentation performance requires direct validation across age groups rather than inference from tissue morphology alone.

Ventricular volume should therefore be systematically considered when interpreting age-related ChP enlargement, as ventricular expansion may influence both the anatomical relationship between the ChP and surrounding structures and the reliability of its MRI-based delineation [19]. Studies should report absolute ChP volume, intracranial-volume-adjusted ChP volume, and ventricular volume, with ChP-to-ventricular-volume ratios considered as complementary measures rather than interchangeable normalization strategies. Statistical adjustment for ventricular volume and sensitivity analyses comparing adjusted and unadjusted associations may help determine whether age-related ChP enlargement is independent of, or closely associated with, ventricular expansion. However, ventricular volume adjustment cannot eliminate partial-volume effects or correct anatomical segmentation errors, and changes in the strength of an association after adjustment should not automatically be interpreted as evidence of confounding.

4. MRI Acquisition and Choroid Plexus Segmentation

4.1. Image Contrast and Anatomical Target Definition

Three-dimensional T1-weighted acquisitions are commonly used for ChP segmentation because of their widespread availability in clinical and research neuroimaging protocols and compatibility with established processing pipelines [30]. However, ChP signal intensity is not spatially uniform, and its contrast relative to adjacent CSF and ventricular structures may vary according to tissue composition and acquisition characteristics. T2-weighted and fluid-attenuated inversion recovery (FLAIR) acquisitions provide complementary contrast information that may facilitate identification of ChP tissue that is difficult to distinguish on T1-weighted images alone. The segmentation target must therefore be defined before an algorithm is selected: atrial glomus, complete lateral ventricular ChP, and all ventricular compartments are not interchangeable anatomical measures.

Standardization of MRI acquisition is essential for reproducible ChP volumetry. Native spatial resolution, including voxel dimensions and slice thickness, and sequence-dependent tissue contrast have particularly direct implications for boundary delineation and partial-volume effects. Magnetic field strength influences signal-to-noise ratio and susceptibility contrast, while contrast-agent administration may alter ChP visibility and segmentation boundaries [3,31]. However, the relative impact of these factors depends on the acquisition protocol and segmentation method, and current evidence does not support a universal minimum spatial resolution or field strength. At a minimum, studies should report scanner manufacturer and model, field strength, MRI sequence, native voxel dimensions, slice thickness, repetition and echo times, inversion time when applicable, and contrast-agent administration details. Native and resampled resolutions should be distinguished. Multicenter and longitudinal investigations should maintain consistent acquisition protocols whenever feasible, document scanner or protocol changes, and assess site-dependent variability through harmonization procedures, scan–rescan measurements, and sensitivity analyses. Reporting test–retest reliability and volumetric bias across acquisition conditions would further support interstudy comparability and interpretation of longitudinal changes [32].

4.2. Manual Annotations and Reference Standards

Manual segmentation has traditionally served as a reference approach for evaluating automated ChP delineation because it permits direct inspection of individual MRI slices and adjustment of boundaries according to recognizable anatomical landmarks. However, manual annotations remain dependent on image quality, operator expertise, and the anatomical criteria used to determine whether ambiguous voxels should be included or excluded. A comprehensive manual segmentation protocol based on 3D Slicer provides separate regions of interest for the right and left lateral ventricular ChP and the ChP of the third and fourth ventricles. The protocol combines axial, coronal, and sagittal inspection to distinguish ChP tissue from surrounding ventricular CSF, the fornix, thalamus, hippocampal region, and posterior fossa structures. The protocol also highlights the difficulty of delineating the smaller third and fourth ventricular components using conventional MRI [1].

For practical MRI segmentation, anatomical boundaries should be operationally defined using reproducible landmarks and verified across sagittal, axial, and coronal planes. In the third ventricle, delineation should focus on the ChP associated with the ventricular roof, using the foramen of Monro, fornix, and thalamus as anatomical landmarks while carefully excluding adjacent internal cerebral veins, parenchyma, and CSF. In the fourth ventricle, segmentation should follow the visible ChP arising from the inferior ventricular roof, with reference to the pons, medulla, inferior medullary velum, and cerebellar structures. Particular attention is required near the median and lateral apertures, where the protocol should explicitly define whether ChP extensions beyond the ventricular cavity are included. When tissue boundaries cannot be reliably distinguished, uncertain voxels should be handled according to predefined inclusion criteria rather than inferred anatomical continuity. These procedures provide operational MRI boundaries without implying histological accuracy [1].

Other validation studies have employed more restricted manual delineation procedures. One validation study generated reference annotations from non-contrast-enhanced T1-weighted images using ITK-SNAP, focusing on the lateral ventricular ChP and including its visible temporal horn extension [33]. In contrast, another investigation used coregistered T1-weighted, T2-weighted, and FLAIR images to generate manually approved reference masks concentrated in the atrial regions. These differences demonstrate that manually segmented ChP volumes are not necessarily anatomically equivalent across studies, even when generated by trained observers [3]. Interobserver agreement introduces an additional

source of uncertainty. One study reported an overall intraclass correlation coefficient of 0.73 among three raters in a subsample of 10 participants, indicating measurable variability in manual delineation. Similarly, a separate investigation documented differences between manual annotations in a clinical validation dataset, emphasizing that expert-generated reference masks are themselves subject to measurement variability [33]. Manual annotations are operational reference standards, not independent confirmation of complete anatomical validity. Their interpretation depends on the ventricular compartments included, image quality, and rules for ambiguous voxels.

4.3. Atlas-Based and Probabilistic Methods

Atlas-based approaches estimate anatomical labels by combining image registration, probabilistic anatomical information, and tissue-dependent image characteristics. FreeSurfer provides automated ChP labels within its subcortical segmentation framework and has been widely used in volumetric investigations. However, validation studies have identified discrepancies between FreeSurfer-derived labels and expert manual segmentations, particularly in regions characterized by irregular morphology and heterogeneous image contrast [3]. Conventional FreeSurfer ChP labels chiefly cover the lateral ventricular components; they should not be described as whole-ChP volume without qualification.

To improve segmentation, a Gaussian mixture model (GMM)-based method was introduced to distinguish ChP tissue from adjacent structures using probabilistic image-intensity characteristics. The approach improved correspondence with manual reference segmentations compared with conventional FreeSurfer output, although performance varied across the investigated datasets and clinical populations. These findings supported the potential value of image-specific tissue classification while demonstrating that segmentation accuracy remains dependent on anatomical and acquisition-related variability [30]. A subsequent study developed a region-informed GMM approach incorporating anatomical priors derived from FreeSurfer-defined lateral ventricular and ChP regions. The method was evaluated in 38 participants, including 19 cognitively normal individuals, 11 with mild cognitive impairment, and eight with Alzheimer's disease. Using manually defined ChP masks as the reference, the proposed model achieved a mean Dice similarity coefficient of 0.82 ± 0.05, compared with 0.24 ± 0.11 for FreeSurfer and 0.66 ± 0.10 for the previously established two-stage GMM approach [34]. The model nevertheless slightly underestimated manual ChP volume. Its small development cohort and restricted acquisition setting limit generalization across scanners and populations.

4.4. Deep Learning-Based Methods

Deep learning approaches have increasingly been developed to address limitations of conventional atlas-based ChP segmentation. Convolutional neural networks can learn spatial and image-intensity patterns from manually annotated examples, reducing the need for extensive operator intervention once a model has been trained. However, the anatomical scope and performance of these methods remain dependent on the training annotations, dataset composition, and validation procedures. A two-stage three-dimensional U-Net approach was developed for lateral ventricular ChP segmentation from T1-weighted MRI, while minimizing preprocessing requirements. The model was developed using research datasets including healthy controls and patients with multiple sclerosis and subsequently evaluated using clinical MRI from individuals with radiologically isolated syndrome. The authors reported mean Dice coefficients of 0.72 ± 0.01 in the research dataset and 0.67 ± 0.01 in the clinical dataset, with corresponding correlations between predicted and manually delineated volumes of 0.86 and 0.84 [33].

Three sequence-specific fully convolutional models were trained on MRI datasets from 50 participants, including healthy individuals and patients with neurodegenerative conditions. The reported Dice coefficients were 0.72 for T1-weighted images, 0.72 for T2-weighted images, and 0.74 for FLAIR images, with 95th-percentile Hausdorff distances of 1.97, 2.22, and 1.69 mm, respectively. Although the models outperformed FreeSurfer under the investigated conditions, the reference annotations were concentrated in the lateral ventricular atria, restricting conclusions about their ability to recover the complete anatomical extent of the ChP [3]. ASCHOPLEX combines several deep learning architectures, including 3D U-Net, UNETR, and DynUNet. The system was initially developed using 128 T1-weighted MRI scans from healthy controls and patients with multiple sclerosis, while a fine-tuning strategy was evaluated using 77 PET/MRI-derived datasets including controls and patients with depression. The investigators reported Dice coefficients of 0.80 for the original framework and 0.78 for the fine-tuned implementation, with estimated volumetric errors of approximately 9.2% in both settings. These findings support the feasibility of model adaptation across imaging datasets, although performance estimates remain specific to the anatomical annotations and acquisition conditions evaluated [35].

Another approach trained a deep neural patchwork model using manually segmented contrast-enhanced MRI datasets. The investigation included 199 patients undergoing imaging before stereotactic procedures, with 149 datasets used for model development and 50 for testing. The model achieved a mean Dice coefficient of 0.81 $\pm$ 0.05 on contrast-enhanced T1-weighted images, compared with 0.71 $\pm$ 0.05 and 0.70 $\pm$ 0.05 when applied to non-contrast T1-weighted and T2-weighted images, respectively. FreeSurfer achieved a Dice coefficient of 0.38 $\pm$ 0.05 in the same comparison. These results demonstrate the potential value of contrast-enhanced reference imaging for model development but do not establish complete anatomical coverage or histological correspondence [31]. An important limitation in comparing these studies is that their reported Dice coefficients arise from different datasets, reference annotations, anatomical regions, and acquisition protocols. Consequently, performance estimates cannot be interpreted as a direct ranking of segmentation methods unless they are obtained under comparable evaluation conditions. The Metrics Reloaded framework further indicates that validation metrics must be selected according to the characteristics of the target structure and the intended application [36]. Table 1 summarizes representative MRI-based ChP segmentation methods, highlighting their anatomical coverage, reference annotations, and reported validation outcomes.

Table 1. Anatomical scope and validation of representative MRI-based choroid plexus segmentation methods.

Study/Design	MRI Inputs and Segmentation Strategy	Reference Anatomy and Dataset	Reported Quantitative Finding	Scope of Supported Inference
Bannai et al. (2023) [1]	3D T1-weighted MRI; multiplanar expert tracing in 3D Slicer.	Separate right/left lateral, third- and fourth-ventricle masks; region-specific exclusion landmarks.	Anatomical annotation protocol; not a head-to-head algorithmic Dice benchmark.	Broader ventricular coverage is feasible manually, but MRI-based annotations are not histological boundary measurements.
Tadayon et al. (2020) [30]	T1-weighted MRI; Gaussian mixture refinement of FreeSurfer ChP labels.	Manual comparators in contrast-enhanced ($n = 19$), healthy ($n = 20$), and AD ($n = 20$) datasets.	Dice improvement over FreeSurfer: ΔDice ≈ 0.20 in the contrast-enhanced-reference comparison.	Demonstrates improved agreement with manual labels, not independent verification of whole-ventricular coverage.

Table 1. *Cont.*

Study/Design	MRI Inputs and Segmentation Strategy	Reference Anatomy and Dataset	Reported Quantitative Finding	Scope of Supported Inference
Yazdan-Panah et al. (2023) [33]	Non-contrast 3D T1-weighted MRI; coarse-to-fine segmentation.	Bilateral lateral-ventricle ChP through the visible temporal horn; third/fourth ventricles excluded.	Dice 0.72 ± 0.01 (research) and 0.67 ± 0.01 (clinical); volume r = 0.86/0.84.	Clinical-domain testing supports transfer within a lateral-ventricular target, with lower performance on routine scans.
Storelli et al. (2024) [37]	3-T T1-weighted and FLAIR MRI; sequential intensity-model classification.	Manual ChP masks in 55 people with MS and 60 controls; comparisons with FreeSurfer and FS-GMM.	Dice 0.65 ± 0.06 vs. 0.37 ± 0.08 (FreeSurfer) and 0.58 ± 0.06 (FS-GMM).	Within-cohort advantage depends on paired sequences and the particular manual definition and population.
Eisma et al. (2024) [3]	3D T1, 3D T2 and 2D T2-FLAIR; independent convolutional models.	Expert annotations concentrated in the lateral-ventricular atria (n = 50 development); n = 98 separate lifespan cohort.	Dice 0.72 (T1), 0.72 (T2), 0.74 (FLAIR); FreeSurfer 0.19 in their benchmark.	Strong atrial-mask concordance does not validate temporal, third- or fourth-ventricle completeness.
Visani et al. (2024) [35]	T1-weighted MRI; 3D U-Net/UNETR/ DynUNet with domain fine-tuning.	Expert manual labels; 128 initial MRI scans and 77 PET/MRI scans for adaptation.	Dice 0.80 (initial) and 0.78 (fine-tuned); estimated volume error 9.22%/9.23%.	Domain adaptation is demonstrated; anatomical equivalence to other studies was not tested under a shared reference.
Zhou et al. (2025) [34]	Anatomical priors from FreeSurfer plus intensity clustering.	Manual reference; 38 analysed participants: 19 cognitively normal, 11 MCI, 8 AD.	Dice ≈ 0.82 vs. 0.24 (FreeSurfer) and 0.66 (Two-GMM); lower estimated volume than manual.	Improved overlap can coexist with a systematic downward shift in estimated volume.
Incesoy et al. (2026) [31]	Contrast-enhanced/postcontrast T1 training; transfer to non-contrast T1 and T2.	Contrast-enhanced lateral-ventricle manual masks; 199 patients (149 train, 50 test).	Dice 0.81 ± 0.05 (postcontrast T1), 0.71 ± 0.05 (non-contrast T1), 0.70 ± 0.05 (T2).	Contrast-derived labels aid non-contrast segmentation, but enhancement is not a histological definition.

Abbreviations: AD, Alzheimer's disease; ChP, choroid plexus; FLAIR, fluid-attenuated inversion recovery; FS, FreeSurfer; GMM, Gaussian mixture model; MCI, mild cognitive impairment; MS, multiple sclerosis. Numerical results are as reported by each study, not harmonized across datasets. The final column is an evidence-bounded interpretation by the review authors, not an outcome independently tested in every study.

4.5. Interpreting Segmentation Performance Metrics

Segmentation studies commonly quantify performance using spatial overlap metrics, boundary distances, and volumetric agreement. The Dice similarity coefficient measures overlap between a predicted segmentation and a reference annotation, whereas the 95th-percentile Hausdorff distance characterizes boundary discrepancies while reducing sensitivity to isolated extreme deviations. Volume-based measures, including relative volume differences and intraclass correlation coefficients, provide complementary information about measurement agreement or reliability but address questions that differ from voxel-level anatomical correspondence. The ChP's thin extensions and folded surfaces make overlap metrics sensitive to small boundary displacements. Conversely, similar total volumes can conceal regional omissions or inclusion of adjacent tissue. The Metrics Reloaded framework emphasizes that image-segmentation validation should employ complementary metrics selected according to the characteristics of the target structure and the intended application.

For ChP volumetry, spatial overlap, boundary distances, and volumetric bias characterize segmentation accuracy relative to an imaging reference, whereas regional completeness and correspondence with established neuroanatomical boundaries address anatomical validity [36]. Neither dimension establishes biological validity, which requires independent evidence linking MRI-derived measurements to specific tissue characteristics or physiological processes [36]. Independent validation should test robustness to scanner characteristics, spatial resolution, preprocessing, demographic variation, and disease-associated changes in ventricular anatomy.

5. Anatomical and Technical Sources of Measurement Error

5.1. Anatomical and Technical Sources of Error

At the ChP attachment, MRI often cannot resolve the histological transition to neighboring tissue. Protocols should therefore state how ambiguous boundary voxels are handled and whether the target is the visible ChP, a predefined subregion, or the complete anatomically recognizable structure. Partial-volume effects arise when a voxel contains ChP together with CSF or adjacent parenchyma. They are especially consequential at thin folds and narrow ventricular extensions. Mixed-tissue voxels are a recognized cause of uncertainty in MRI segmentation more generally, particularly where structures have thin or highly folded boundaries [38]. Their magnitude depends on native resolution, slice orientation, and sequence contrast. Comparable performance within the annotated atrial region does not demonstrate equivalent accuracy in smaller ChP extensions or other ventricles. Partial-volume effects can cause either overestimation, through inclusion of CSF-containing boundary voxels, or underestimation, through exclusion of incompletely resolved ChP tissue. Resampling cannot recover information absent from the native acquisition. Studies should report native voxel dimensions separately from any resampled resolution used by the algorithm.

T1-weighted, T2-weighted, FLAIR, and contrast-enhanced acquisitions define ChP boundaries with different tissue contrast. Similar aggregate overlap scores need not indicate identical local anatomical boundaries. Contrast enhancement reflects vascular and contrast-agent properties, not the epithelial basement membrane or histological margins. An enhancement-defined segmentation is therefore an imaging reference, not histological validation. Preprocessing can introduce further variability. Registration, intensity normalization, skull stripping, bias-field correction, and spatial resampling may influence the image features subsequently used for segmentation. a multi-sequence study developed a segmentation method combining T1-weighted and FLAIR images with Gaussian mixture modeling, while other work investigated a deep learning framework incorporating model adaptation across imaging datasets. These approaches illustrate how differences in image processing and classification may influence the resulting segmentation [37]. Comparisons between ChP pipelines should account for registration, intensity correction, resampling, and image classification rather than attributing volume differences to biology alone.

Calcification can alter MRI signal, but whether it leads to false inclusion or exclusion of ChP voxels is sequence- and method-dependent; systematic measurement bias cannot be assumed. Segmentation protocols should specify whether a mask represents the ChP's outer anatomical envelope or only tissue classified within that envelope, particularly when cystic components are present. However, ventricular enlargement should not be assumed to reduce segmentation accuracy in every imaging framework. One validation study specifically examined the relationship between lateral ventricular volume and segmentation performance. Ventricular volume was not significantly associated with Dice coefficients for the T1-weighted, T2-weighted, or FLAIR models, although a borderline positive association was observed with the 95th-percentile Hausdorff distance for the T1-weighted model

($p = 0.050$). These findings suggest that the investigated algorithms maintained relatively stable segmentation performance across different ventricular sizes, despite the underlying anatomical variability [3]. Ventricular enlargement is therefore a possible source of anatomical uncertainty, not a demonstrated universal cause of segmentation error. Its effect should be measured for each pipeline. Age-stratified validation should evaluate regional segmentation errors and volume bias, even when overall Dice coefficients are similar across age groups.

Disease-related anatomical alterations represent an additional potential source of segmentation bias. In neurodegenerative disorders, cerebral atrophy, ventricular enlargement, and changes in tissue composition may differentially affect ChP boundary identification in patients and healthy controls. Consequently, apparent between-group differences in ChP volume may partly reflect systematic segmentation errors rather than underlying biological changes. To address this possibility, segmentation accuracy and signed volumetric bias should be independently evaluated in clinical and control populations using appropriate reference annotations. Disease-specific validation should include regional error analyses, particularly in the atrial glomus and thinner ventricular extensions, to identify potential systematic overestimation or underestimation. Such analyses are necessary to determine whether segmentation performance remains comparable across diagnostic groups before attributing volumetric differences to disease-related ChP alterations.

5.2. Repeatability and Measurement Uncertainty

Agreement with expert-drawn masks can inherit their anatomical omissions or inclusion rules. Differences from a manual mask do not establish the anatomical source of an error without further evaluation. Recent evidence also highlights the importance of distinguishing cross-sectional agreement from longitudinal measurement reliability. Rusinek et al. assessed the test–retest reliability of FreeSurfer 7.1 measurements in 100 older adults who underwent two 3-T MRI examinations on the same scanner, separated by a mean interval of 5.5 weeks. The study identified relatively low reliability for ChP volumetry compared with several larger and more anatomically compact brain structures. Longitudinal FreeSurfer processing improved measurement precision, but the ChP remained a challenging target for detecting small within-person changes [32]. For detection of a 1% within-person difference with 80% power, the investigators estimated sample sizes of approximately 1018 using cross-sectional FreeSurfer processing and 633 using longitudinal processing. These estimates apply to the studied pipeline and acquisition conditions. General guidance for quantitative imaging biomarkers likewise distinguishes repeatability, reproducibility, and the minimum change detectable beyond measurement error [39].

Storelli et al. found that the estimated associations between ChP volume and disability in multiple sclerosis differed according to the segmentation method used, illustrating the potential clinical consequences of pipeline choice. These findings support evaluating measurement uncertainty before interpreting relatively small volumetric differences as evidence of neurodegenerative change. Reliable ChP volumetry requires evidence of spatial agreement, limited systematic bias, acceptable repeatability, and stability across the imaging conditions and populations relevant to the intended application [37]. Table 2 summarizes the main anatomical and methodological sources of uncertainty in MRI-derived ChP volumetry, distinguishing the findings supported by available evidence from interpretations that remain insufficiently validated.

Table 2. Evidence-to-inference audit for anatomical threats to choroid plexus MRI volumetry.

Anatomical or Measurement Issue	Direct Observation from Original study	Implication for the MRI-Derived Quantity	Inference That Remains Unsupported
Ventricular compartment mismatch	Manual delineation permits four separately labelled ventricular components; atrium-restricted references have also been used [1,3].	Lateral-atrial and whole-ventricular segmentations sample different anatomical territories.	An atrial ChP volume should not be presented as complete whole-ChP volume.
Manual-reference uncertainty	In the clinical dataset, agreement between manual annotators was Dice 0.64 ± 0.02 [33].	Algorithm–manual overlap is bounded by annotation visibility and observer consistency.	Agreement with one MRI reference mask is not direct histological validation.
Partial-volume handling and erosion	Region-informed One-GMM achieved Dice ≈ 0.82 but underestimated manual ChP volumes; boundary erosion was discussed as a possible contributor [34].	Suppressing mixed CSF/tissue boundary voxels can change the numerical volume even as spatial overlap improves.	Improved Dice does not establish unbiased volume or recovery of all thin ChP extensions.
MRI contrast dependence	The same deep model achieved Dice 0.81 on contrast-enhanced T1, 0.71 on native T1, and 0.70 on T2 [31].	Boundary detectability differs by acquisition contrast under an otherwise shared reference.	An enhanced MRI label cannot be equated with microscopic epithelial or stromal limits.
Vascular versus total-tissue volume	At 7 T, older subjects had lower ChP vascular density (16.5 ± 4.34% vs. 24.85 ± 6.84%; $n = 49$) [2].	Apparent total-volume change may coexist with an opposing change in vascular fraction.	Total ChP volume is not a direct measure of vascular mass or epithelial hypertrophy.
Calcification versus bulk ChP	CT calcium burden and MRI ChP volume were analysed separately in $n = 166$; QSM/CT calcification volumes correlated r = 0.728 ($n = 22$) [27,28].	Mineralized ChP components are independently measurable and need not track total volume identically.	Neither QSM calcification volume nor bulk MRI volume establishes tissue-specific cellular change.
Cystic tissue inclusion	Multisequence 7-T MRI identified ChP cysts; cyst number and size correlated with ChP volume, with greater burden in the AD group [29].	A contour enclosing cystic regions may capture a different tissue mixture from a solid-tissue mask.	Increased volume alone cannot distinguish cystic contribution from epithelial or stromal growth.
Ventriculomegaly and aging	Both lateral-ventricle and ChP volumes increased with age ($n = 155$); ventricular size was not significantly associated with Dice in three tested CNN models [3,19].	The local ChP environment changes with age, but a universal loss of segmentation accuracy with ventricle size is not demonstrated.	Ventricular enlargement should not be labelled a proven segmentation error without method-specific analysis.
Short-interval measurement reliability	In 100 older adults scanned twice, FreeSurfer 7.1 showed low ChP repeatability; detecting 1% change in whole-ChP volume required $n \approx 1018$ (cross-sectional) or 633 (longitudinal) [32].	Test–retest noise can exceed changes in interest; processing choices modify power.	Cross-sectional Dice or group-level associations cannot establish individual longitudinal detectability.

The first two columns distinguish source-reported observations from anatomy-specific implications; the last column states what the cited evidence does not establish. The latter two columns are the authors' critical synthesis, not results of new experiments. Abbreviations: AD, Alzheimer's disease; ChP, choroid plexus; CNN, convolutional neural network; CT, computed tomography; CSF, cerebrospinal fluid; QSM, quantitative susceptibility mapping. The Rusinek et al. power estimates apply specifically to the investigated FreeSurfer 7.1/3-T repeat-scan setup.

6. Clinical Interpretation in Cognitive Aging and Neurodegeneration

6.1. Changes Associated with Aging Versus Disease

The interpretation of magnetic resonance imaging (MRI)-derived choroid plexus (ChP) volume in neurodegenerative diseases is complicated by the substantial morphological variability already present during physiological aging. Normative MRI investigations have demonstrated age-associated ChP enlargement, indicating that increased volume is not inherently specific to neurodegenerative pathology [3]. Moreover, human postmortem transcriptomic analyses have identified age-related molecular changes in the ChP, with particularly pronounced differences between individuals in their fifth and sixth decades of life [40]. These observations suggest that structural and molecular changes may occur independently of clinically apparent cognitive impairment. Age-related ChP alterations are also observed in individuals without dementia. In the IGNITE cohort, a population-based study investigated 635 cognitively unimpaired older adults and found that greater ChP volume was associated with smaller hippocampal and gray matter volumes and larger ventricular volumes. Poorer self-reported sleep quality was also associated with greater ChP volume, whereas corresponding associations were not observed for accelerometry-derived sleep measures. These findings illustrate that ChP volumetry may reflect a combination of aging-related, behavioral, and structural characteristics even in the absence of diagnosed neurodegenerative disease [41]. Disease-group differences therefore require adjustment for age, cranial and ventricular size, and segmentation method; they cannot automatically be attributed to disease-specific ChP remodeling. This distinction becomes particularly relevant in mild cognitive impairment (MCI), which encompasses clinically and biologically heterogeneous conditions. An increase in ChP volume among individuals with MCI may occur in association with Alzheimer's disease (AD) pathology, but clinical classification alone does not identify the specific biological process responsible for the observed morphological difference [42].

6.2. Choroid Plexus Volume Across the Alzheimer's Disease Continuum

Accumulating MRI evidence indicates that ChP volume is frequently greater in individuals with AD than in cognitively unimpaired controls. A systematic review including 16 studies, comprising 2004 patients with AD and 883 healthy controls, identified a pooled standardized mean difference of 1.05 (95% confidence interval, 0.67–1.43) in a meta-analysis of six eligible studies, consistent with greater ChP volume in AD [5]. However, substantial heterogeneity in participant characteristics, imaging protocols, and segmentation approaches complicates the interpretation of this pooled association as a uniform anatomical effect. In a retrospective cohort comprising 203 individuals across the AD continuum and 82 healthy controls, an observational cohort study reported greater ChP volume in the AD group than in controls. However, ChP volumes did not differ significantly between the AD non-dementia and dementia subgroups. Within the AD continuum, greater volume was associated with greater global amyloid-β (Aβ) deposition, poorer memory and executive performance, and greater clinical impairment. These results indicate that ChP enlargement may accompany AD-associated abnormalities, but they do not establish a monotonic relationship between volume and clinical disease stage [43].

A prospective imaging investigation examined 607 participants from the Chinese Imaging, Biomarkers, and Lifestyle cohort, including 110 healthy controls, 269 individuals with MCI, and 228 patients with AD dementia. Participants with AD dementia exhibited greater baseline ChP volume than the other groups. Larger ChP volume was associated with lower cerebrospinal fluid (CSF) Aβ concentrations, poorer cognitive performance, greater neuropsychiatric symptom burden, and alterations in cognition-related brain structures. These associations persisted in models accounting for demographic characteristics, APOE

ε4 status, estimated total intracranial volume, and hippocampal volume [42]. Beyond these adjusted associations, the addition of ChP volume to hippocampal volume improved diagnostic discrimination compared with hippocampal volume alone. For example, the AUC for distinguishing AD dementia from MCI increased from 0.843 to 0.863 ($p = 0.008$). Improved discrimination was also reported for cerebral Aβ42 alterations and other diagnostic comparisons. However, these findings do not establish incremental value beyond comprehensive models incorporating amyloid, tau, and clinical biomarkers [42].

In a larger UK Biobank analysis involving 45,306 participants, investigators identified associations between greater ChP volume, lower ChP MRI signal intensity, cognitive impairment, and incident dementia. The population-based design provides evidence that ChP imaging characteristics may be relevant beyond highly selected memory-clinic cohorts. Nevertheless, automatically generated structural measurements and observational clinical outcomes do not establish that changes in ChP morphology are specific to AD or represent a direct measure of blood–CSF barrier dysfunction [6].

6.3. Mild Cognitive Impairment and Longitudinal Progression

The potential relevance of ChP volumetry during prodromal disease has been investigated using longitudinal cohorts and classification models. One study examined Alzheimer's Disease Neuroimaging Initiative (ADNI) data from 453 individuals with MCI, including 115 who subsequently progressed to AD dementia and 338 who remained clinically stable. The progressive-MCI group exhibited greater right ChP volume than the stable-MCI group. However, prediction was improved by combining ChP measurements with auditory verbal learning performance, highlighting the importance of evaluating volumetry within a broader clinical framework [44]. Longitudinal changes have also been reported in cohorts spanning several stages of cognitive impairment. a separate investigation analyzed 2334 MRI observations from 613 ADNI participants and found an overall increase in ChP volume over time. The longitudinal trajectory varied according to sex, cognitive decline, and APOE ε4 status, suggesting that demographic and biological characteristics may influence the interpretation of within-person volumetric change [22].

In a prospective cohort, ChP volume was associated with baseline cognitive and functional measures, while more rapid enlargement was associated with worsening neuropsychiatric symptoms during follow-up. These findings provide preliminary longitudinal evidence, although the relatively short follow-up interval and observational design limit conclusions about the temporal ordering of ChP remodeling and clinical deterioration [42]. More recent work has moved beyond total volume. A longitudinal study investigated higher-order ChP morphological features in 564 participants without dementia from ADNI, relating imaging-derived characteristics to amyloid and tau positron emission tomography (PET) measures and subsequent cognition. Their findings suggest that regional shape and morphological complexity may capture information not represented by total ChP volume alone [4].

Evidence for incremental predictive value is also emerging from ChP radiomics studies. Yin et al. compared clinical-only, ChP radiomics-only, and combined models, reporting AUCs of 0.809, 0.794, and 0.907, respectively, for distinguishing MCI from AD. For predicting MCI-to-AD progression, the corresponding AUCs were 0.776, 0.745, and 0.900. Adding the ChP radiomics score to the clinical model also improved discrimination and reclassification, with an integrated discrimination improvement of 0.065 and a net reclassification improvement of 0.280 [45]. However, these results concern multifeature radiomic signatures rather than ChP volume alone. Their incremental value beyond comprehensive models incorporating hippocampal volume, amyloid and tau biomarkers, and established clinical measures remains insufficiently established. Further externally validated comparisons, including

calibration and clinically relevant performance measures, are needed before statistically significant improvements can be interpreted as meaningful clinical utility.

6.4. Amyloid, Tau, and Complementary Imaging Markers

Multimodal investigations have explored whether ChP morphology is associated with established AD biomarkers. One AD-continuum cohort reported a positive association between ChP volume and global amyloid PET burden after adjustment for age and sex [43]. A separate cohort identified associations between ChP volume and CSF Aβ concentrations, together with relationships involving cognitive and neuroanatomical measures. These findings link MRI-derived ChP morphology with established AD-related biomarkers but do not identify the cellular mechanisms responsible for the associations [42]. A complementary study jointly examined ventricular volume, ChP volume, and ventricular PET radioactivity in 385 participants from the TRIAD cohort and 282 from ADNI. The investigators reported associations among these imaging measures and with amyloid PET, tau-related fluid biomarkers, glial fibrillary acidic protein, and cognition. These findings support evaluating ChP volumetry as one component of a broader choroidal–ventricular imaging phenotype rather than an isolated proxy for CSF clearance [46].

Investigations combining diffusion MRI and ChP volumetry provide further evidence of relationships between ChP enlargement and brain microstructural abnormalities. A multimodal MRI analysis included 1351 cognitively impaired ADNI participants using automatically segmented ChP volume, peak width of skeletonized mean diffusivity (PSMD), diffusion tensor imaging analysis along the perivascular space (DTI-ALPS), and the neutrophil-to-lymphocyte ratio. Larger ChP volume was associated with greater white matter microstructural abnormalities, lower DTI-ALPS indices, higher inflammatory ratios, and poorer cognitive performance [47]. A separate study of 188 participants reported greater ChP and CSF volumes and lower DTI-ALPS indices in patients with AD than in groups with MCI, subjective cognitive decline, or normal cognition. Although statistical mediation analyses suggested interrelationships among these imaging measurements, their observational nature does not establish a causal pathway in which ChP enlargement alters glymphatic drainage [48]. DTI-ALPS and other diffusion-derived proxies describe properties of water diffusion, not direct measurements of glymphatic transport. Associations with ChP volume should not be interpreted as evidence of a causal pathway.

6.5. Biological Interpretation and Its Limitations

Experimental and molecular studies provide biological context for imaging findings, but their results operate at anatomical scales different from those accessible to conventional MRI. Experimental work demonstrated an age-associated type I interferon response in the ChP and showed that experimental modulation of this pathway could influence cognitive and neurogenic outcomes in aged mice [49]. Subsequent work identified altered interferon-related transcriptional responses in the ChP of an experimental AD model. These studies support the biological relevance of ChP immune signaling but do not establish a direct relationship between interferon activity and ChP enlargement measured in patients [50]. Human molecular investigations have also identified heterogeneity within the aging ChP. A human postmortem study reported age-associated transcriptomic differences in postmortem ChP samples [40], while CSF proteomic profiling identified five molecular subtypes of AD through CSF proteomic analyses. The subtype characterized by ChP-related dysfunction exhibited the largest ChP volumes among the identified molecular subgroups. This observation suggests a potential correspondence between molecular and structural phenotypes, but subgroup associations cannot establish that the observed MRI volume increase arises from a particular epithelial or stromal process [51].

More broadly, a large-scale investigation analyzed paired CSF and plasma proteomic data from 2171 healthy or cognitively impaired older individuals and identified age-associated changes in the relative concentrations of numerous proteins across the two compartments. These findings provide evidence of alterations in the molecular environment of the CSF–plasma interface during aging and cognitive impairment. However, they do not isolate the ChP as the anatomical origin of those changes and should not be interpreted as direct validation of MRI-derived ChP volume as a blood–CSF barrier biomarker [52].

6.6. Disease Specificity and Clinical Interpretation

The clinical interpretation of ChP enlargement requires consideration of its occurrence in neurological conditions other than AD. ChP volume alterations have also been investigated in multiple sclerosis, where their relationships with inflammatory activity have motivated studies of potential diagnostic differentiation. An imaging study evaluated 50 participants with multiple sclerosis and 64 with alternative diagnoses and found that normalized ChP volume provided moderate discrimination between multiple sclerosis and its mimics, with AUCs of 0.71 and 0.65 across the two cohorts. These findings demonstrate that ChP volumetric abnormalities are not restricted to AD [53]. A systematic review of 48 studies across neurological and psychiatric conditions found frequent ChP enlargement but insufficient evidence for consistent associations with disease severity [8]. A more recent investigation compared ChP volume fraction and diffusion-derived imaging parameters among patients with AD, Parkinson's disease, idiopathic normal-pressure hydrocephalus, and healthy controls. The inclusion of multiple diagnostic groups illustrates the importance of distinguishing disease-related structural characteristics from alterations shared by neurodegenerative and ventricular disorders. However, differences in sample characteristics and normalization procedures must be considered before interpreting ChP volume as a disease-specific marker [54]. Because the reviewed studies use different segmentation targets and methods, variability in the apparent association between ChP volume and cognitive disease may reflect measurement as well as biological differences. Discrimination within a selected cohort does not establish clinical utility. Proposed ChP biomarkers need external validation, calibrated performance estimates, and evidence that measurement uncertainty is small relative to the changes being interpreted.

7. Recommendations for Standardization and Future Research

Future investigations should explicitly define the ventricular compartments included, anatomical boundaries, and criteria for handling ambiguous tissue interfaces. Reference annotations should ideally be developed through collaboration between neuroanatomists and neuroradiologists, using multiplanar assessment and standardized anatomical landmarks. A published manual segmentation protocol provides an example of compartment-specific anatomical delineation. Nevertheless, interobserver variability and limited tissue contrast prevent expert annotations from being regarded as error-free representations of the underlying anatomy. The CLAIM 2024 Update emphasizes transparent reporting of reference standards, annotation procedures, and associated uncertainty in artificial intelligence-based medical imaging studies [55]. Applying these principles to automated ChP segmentation would improve the interpretation of algorithmic performance and facilitate comparisons among models trained using different anatomical targets.

Multicenter harmonization offers opportunities to reduce technical variability but cannot replace anatomical validation. A multicenter study demonstrated that harmonization can reduce site-related variability in structural brain MRI datasets, while highlighting the risk of data leakage when harmonization is performed before separating training and testing data [56]. A phantom-based investigation also showed that scanner characteristics,

acquisition parameters, and preprocessing procedures affect the reproducibility of MRI-derived radiomic features. Although these findings were not specific to ChP volumetry, they provide relevant methodological considerations for multicenter quantitative imaging [57]. Harmonization should be evaluated on independent data and supplemented by anatomical quality control; statistical adjustment cannot recover omitted ChP tissue or reconcile different ventricular coverage.

Longitudinal reproducibility represents a further challenge. A test–retest study identified relatively low test–retest reliability for FreeSurfer-derived ChP measurements in older adults, indicating that measurement variability may compromise the detection of small within-person changes. A broader analysis of automated brain segmentation showed that differences in scanner field strength can affect volumetric reproducibility. These observations reinforce the need to evaluate acquisition-related measurement uncertainty rather than assuming stable performance across imaging conditions [58]. Longitudinal studies should report test–retest uncertainty, within-subject variation, and thresholds for detectable change before interpreting small serial ChP volume differences as biological progression.

Anatomically annotated multimodal datasets, including high-resolution MRI and complementary tissue-sensitive imaging, could clarify the effects of vascular, mineralized, and cystic components on measured ChP volume. Ex vivo imaging with histological correlation would be valuable where feasible. ChP enlargement on MRI does not itself establish altered CSF production, barrier dysfunction, or epithelial pathology. Such interpretations require convergent physiological or histological evidence.

An Anatomy-Centered Validation and Reporting Framework

We propose four requirements for anatomy-centered ChP volumetry: (1) explicit ventricular target definition and inclusion rules; (2) complementary overlap, boundary, regional-completeness, and volumetric-bias metrics; (3) test–retest and multicenter reliability; and (4) independent biological validation when functional interpretation is intended. These are methodological recommendations, not a validated ChP-specific standard. In practical terms, anatomical validation may follow a three-step procedure. First, the target ventricular compartments and segmentation boundaries should be predefined, including explicit rules for handling thin extensions and ambiguous voxels. Second, compartment-specific reference annotations should be generated through independent multiplanar assessment by trained observers, with interobserver variability documented and disagreements resolved through consensus [1]. Third, segmentation performance should be evaluated using complementary overlap, boundary-distance, and signed volumetric error metrics, alongside regional assessment of anatomical completeness, particularly in the third and fourth ventricles [36]. For clinical and longitudinal applications, these assessments should be extended to independent datasets, relevant diagnostic populations, and repeated acquisitions.

Implementation would benefit from transparent reporting practices developed for quantitative imaging and artificial intelligence. The CLAIM 2024 Update provides recommendations for documenting reference annotations, imaging protocols, and model evaluation in medical imaging AI studies [55]. When ChP-derived measurements are incorporated into diagnostic accuracy studies, STARD-AI offers relevant reporting guidance [59]. Similarly, TRIPOD + AI provides recommendations for studies developing or validating clinical prediction models that incorporate imaging-derived features [60]. These guidelines address different methodological applications and complement, rather than replace, anatomical validation. Figure 2 summarizes the complementary roles of measurement reproducibility and anatomical validity in MRI-derived ChP volumetry, emphasizing the need for independent biological validation before interpreting volumetric measurements as markers of tissue pathology or physiological dysfunction.

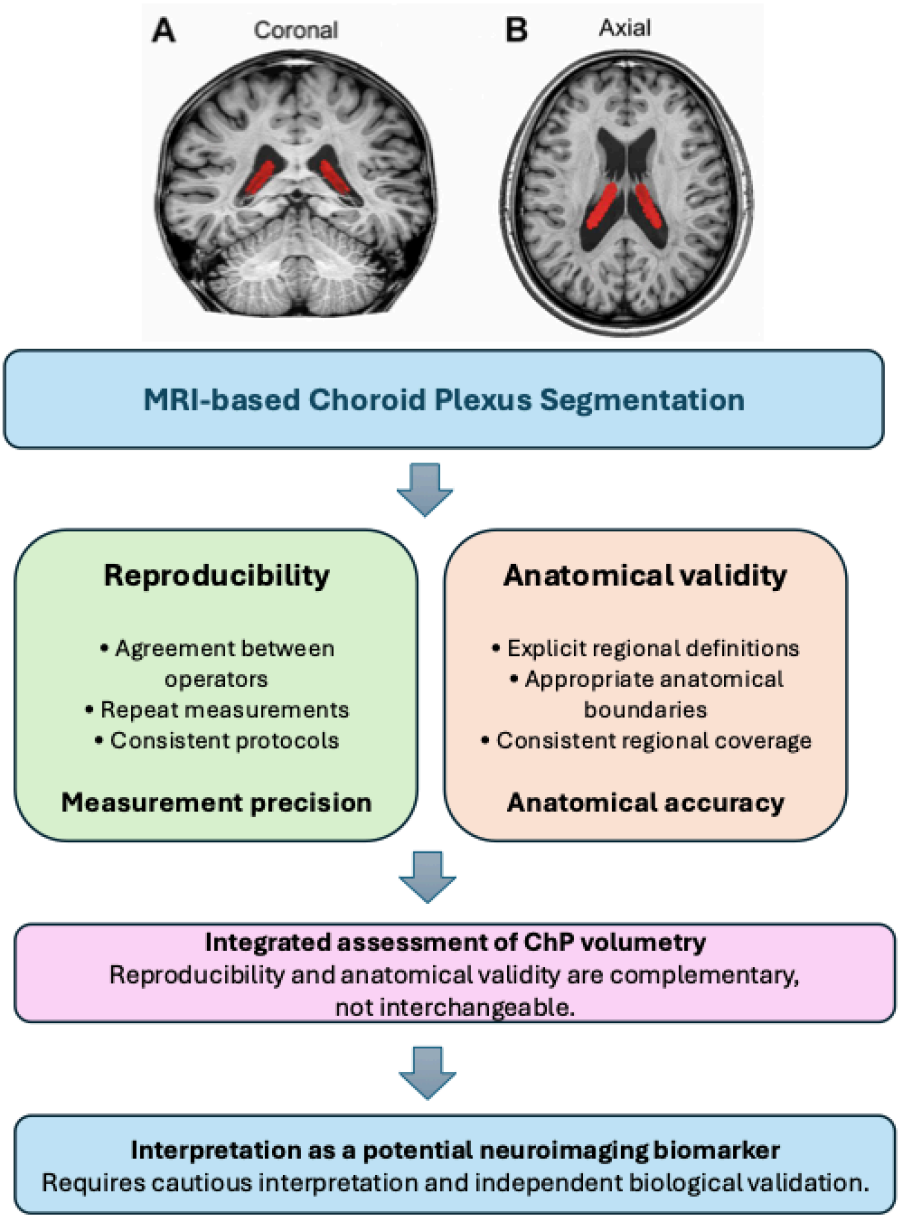


Figure 2. Reproducibility and anatomical validity in MRI-based choroid plexus segmentation. Representative coronal (**A**) and axial (**B**) magnetic resonance images illustrating manual delineation of the choroid plexus (ChP), highlighted in red. The accompanying schematic summarizes two complementary dimensions of MRI-derived ChP volumetry. Reproducibility concerns interobserver agreement, repeated measurements, and consistency of acquisition and processing protocols, whereas anatomical validity requires explicit regional definitions, appropriate anatomical boundaries, and consistent coverage of the targeted ventricular compartments. Measurement precision and anatomical accuracy are distinct properties that must be considered together when evaluating ChP segmentation. Although both contribute to the reliability and interpretation of volumetric measurements, neither establishes the biological specificity of ChP volume as a neuroimaging biomarker. Independent biological validation is required when interpreting volumetric alterations in relation to underlying tissue changes or physiological dysfunction. Image sources and copyright information: MRI panels (**A**,**B**) were adapted from Figure 2B of [34]. Copyright © 2025 Zhou et al. The original publication is distributed under the Creative Commons Attribution 4.0 International License (CC BY 4.0; https://creativecommons.org/licenses/by/4.0/). The MRI panels were cropped, rearranged on a white background, and relabeled. The accompanying conceptual framework, graphical layout, and explanatory elements were developed by the present authors.

Shared reference datasets should cover lateral, third, and fourth ventricular ChP, diverse age groups, and relevant neurological populations. Validation across sites is then needed to test whether these definitions improve the comparability of measured volumes. Until such standards are established, ChP volume is best regarded as an imaging-defined morphological measure whose clinical interpretation depends on the segmented anatomy and the performance of the measurement pipeline.

To facilitate the practical implementation of the proposed anatomy-centered framework, Table 3 provides a structured reporting checklist for MRI-based ChP volumetry, distinguishing essential methodological information from advanced validation procedures recommended for clinical, longitudinal, and multicenter investigations.

Table 3. Minimum reporting requirements and advanced validation procedures for MRI-based choroid plexus volumetry.

Domain	Essential Reporting	Advanced Validation
Anatomical target	Ventricular coverage (left/right lateral, III, IV) Region-of-interest limits and exclusion rules	Compartment-wise completeness audit Thin-extension and attachment-zone assessment
MRI acquisition	Scanner model, field strength, sequence, contrast use Native voxel size, slice thickness, TR/TE/TI	Cross-sequence and cross-field agreement Multicenter protocol harmonization
Segmentation pipeline	Software or model version, input images Preprocessing, resampling, manual edits, QC	Independent-pipeline replication Site- and diagnosis-stratified quality audit
Reference standard	Reference mask source and annotation protocol Rater number, consensus and boundary rules	Multi-rater agreement High-resolution multimodal anatomical reference
Spatial accuracy	Evaluated regions and reference sample size Dice and HD95, when reference masks exist	Region-specific boundary error maps False inclusion and omission in thin extensions
Volumetric bias	Volume units and normalization denominator Signed and absolute errors, when evaluable	Bland–Altman agreement Bias stratified by age, diagnosis, ventricular size
Repeatability	Scan–rescan sample and interval, if assessed ICC or within-subject CV, if assessed	Inter-scanner and multicenter reproducibility Repeatability limits and detectable change
Clinical applicability	Cohort age, diagnosis and site Protocol changes, missingness and QC failures	Independent clinical-cohort validation Subgroup bias and longitudinal stability

Note. Essential = information to report or explicitly identify as not assessed. Advanced = additional validation according to study design and intended use. CV, coefficient of variation. HD95, 95th-percentile Hausdorff distance. ICC, intraclass correlation coefficient. QC, quality control. TE, echo time. TI, inversion time. TR, repetition time.

Author Contributions: Conceptualization, M.C. and F.S.; methodology, M.C., F.S. and G.A.B.R.; investigation, M.C., F.S., U.G., N.G.R. and S.L.; writing—original draft preparation, M.C.; writing—review and editing, M.C., F.S., U.G., N.G.R., S.L. and G.A.B.R.; visualization, M.C. and F.S.; supervision, G.A.B.R.; project administration, M.C. All authors have read and agreed to the published version of the manuscript.

Funding: This research received no external funding.

Institutional Review Board Statement: Not applicable.

Informed Consent Statement: Not applicable.

Data Availability Statement: No new data were created or analyzed in this study. Data sharing is not applicable to this article.

Conflicts of Interest: The authors declare no conflicts of interest.

Abbreviations

The following abbreviations are used in this manuscript:

AD	Alzheimer's disease
ADNI	Alzheimer's Disease Neuroimaging Initiative
AI	Artificial intelligence
APOE	Apolipoprotein E
AUC	Area under the receiver operating characteristic curve
CBF	Cerebral blood flow
ChP	Choroid plexus
CNN	Convolutional neural network
CNS	Central nervous system
CSF	Cerebrospinal fluid
CT	Computed tomography
DTI-ALPS	Diffusion tensor imaging analysis along the perivascular space
FLAIR	Fluid-attenuated inversion recovery
GMM	Gaussian mixture model
MCI	Mild cognitive impairment
MRI	Magnetic resonance imaging
MS	Multiple sclerosis
PET	Positron emission tomography
PSMD	Peak width of skeletonized mean diffusivity
QSM	Quantitative susceptibility mapping

References

1. Bannai, D.; Cao, Y.; Keshavan, M.; Reuter, M.; Lizano, P. Manual Segmentation of the Human Choroid Plexus Using Brain MRI. *JoVE* **2023**, 65341. [CrossRef] [PubMed]
2. Sun, Z.; Li, C.; Muccio, M.; Jiang, L.; Masurkar, A.; Buch, S.; Chen, Y.; Zhang, J.; Haacke, E.M.; Wisniewski, T.; et al. Vascular Aging in the Choroid Plexus: A 7T Ultrasmall Superparamagnetic Iron Oxide (USPIO)-MRI Study. *Magn. Reson. Imaging* **2024**, *60*, 2564–2575. [CrossRef] [PubMed]
3. Eisma, J.J.; McKnight, C.D.; Hett, K.; Elenberger, J.; Han, C.J.; Song, A.K.; Considine, C.; Claassen, D.O.; Donahue, M.J. Deep Learning Segmentation of the Choroid Plexus from Structural Magnetic Resonance Imaging (MRI): Validation and Normative Ranges across the Adult Lifespan. *Fluids Barriers CNS* **2024**, *21*, 21. [CrossRef] [PubMed]
4. Lin, M.; Zeng, Q.; Zhong, S.; Nie, S.; Zhang, R.; Hong, H.; Liu, L.; Wang, S.; Li, K.; Luo, X.; et al. Association Between Choroid Plexus Morphological Alterations, Alzheimer Pathologies, and Cognitive Impairment: A Longitudinal Study. *Neurology* **2025**, *105*, e213953. [CrossRef] [PubMed]
5. Mahmoudi, F.; Yazdan Panah, M.; Dehghani Firouzabadi, D.; Vaheb, S.; Ghoshouni, H.; Flores Gonzalez, R.; Shaygannejad, V.; Mirmosayyeb, O. Choroid Plexus Volume in Alzheimer's Disease: A Systematic Review and Meta-Analysis. *J. Alzheimer's Dis.* **2026**, *112*, 53–64. [CrossRef] [PubMed]
6. Yu, T.; Han, X.; Huang, X.; Chang, H.; Liu, X.; Tian, M.; Li, X.; Guo, Y.; Ding, J.; Li, X.; et al. The Choroid Plexus, Cognitive Decline, and Incident Dementia: Insights from the UK Biobank. *Mol. Psychiatry* **2026**, *31*, 6762–6773. [CrossRef] [PubMed]
7. Youh, R.; Perera, C.; Katsiva, C.; Harrison, I.F.; Lythgoe, M.F.; Wright, D.K.; Nizari, S.; Wells, J.A. Evidence for Reduced Choroid Plexus Volume in the Aged Brain. *Fluids Barriers CNS* **2025**, *22*, 97. [CrossRef] [PubMed]
8. Tireli, D.; Christensen, J.R.; Munch, T.N.; MacAulay, N.; Larsson, H.B.W.; Carlsen, J.F.; Cramer, S.P. Choroid Plexus Volume in Brain Disorders: A Systematic Review. *Fluids Barriers CNS* **2025**, *22*, 92. [CrossRef] [PubMed]
9. Vardakis, J.C.; Tully, B.J.; Ventikos, Y. Exploring the Efficacy of Endoscopic Ventriculostomy for Hy-drocephalus Treatment via a Multicompartmental Poroelastic Model of CSF Transport: A Computational Perspective. *PLoS ONE* **2013**, *8*, e84577. [CrossRef] [PubMed]
10. Ghersi-Egea, J.-F.; Strazielle, N.; Catala, M.; Silva-Vargas, V.; Doetsch, F.; Engelhardt, B. Molecular Anatomy and Functions of the Choroidal Blood-Cerebrospinal Fluid Barrier in Health and Disease. *Acta Neuropathol.* **2018**, *135*, 337–361. [CrossRef] [PubMed]
11. Khan, J.; Xu, L.; Tubbs, R.S. The Choroid Plexus. In *Cerebrospinal Fluid and Subarachnoid Space*; Elsevier: Amsterdam, The Netherlands, 2023; pp. 175–192.
12. Koduri, M.M.; Tubbs, R.S. Choroid Plexus of the Fourth Ventricle. In *Cerebrospinal Fluid and Subarachnoid Space*; Elsevier: Amsterdam, The Netherlands, 2023; pp. 193–201.
13. Narra, R.; Burudi, P. Bochdalek Flower Basket Sign. *J. Neurosci. Rural Pract.* **2023**, *15*, 165–166. [CrossRef] [PubMed]

14. Barany, L.; Baksa, G.; Patonay, L.; Ganslandt, O.; Buchfelder, M.; Kurucz, P. Morphometry and Microsurgical Anatomy of Bochdalek's Flower Basket and the Related Structures of the Cerebellopontine Angle. *Acta Neurochir.* **2017**, *159*, 1539–1545. [CrossRef] [PubMed]
15. Xu, H.; Hehnly, C.; Lehtinen, M.K. The Choroid Plexus: A Command Center for Brain-Body Communication during Inflammation. *Curr. Opin. Immunol.* **2025**, *93*, 102540. [CrossRef] [PubMed]
16. Schwerk, C.; Schroten, H. In Vitro Models of the Choroid Plexus and the Blood-Cerebrospinal Fluid Barrier: Advances, Applications, and Perspectives. *Hum. Cell* **2024**, *37*, 1235–1242. [CrossRef] [PubMed]
17. Dani, N.; Herbst, R.H.; McCabe, C.; Green, G.S.; Kaiser, K.; Head, J.P.; Cui, J.; Shipley, F.B.; Jang, A.; Dionne, D.; et al. A Cellular and Spatial Map of the Choroid Plexus across Brain Ventricles and Ages. *Cell* **2021**, *184*, 3056–3074.e21. [CrossRef] [PubMed]
18. Murakami, R.; Chiba, Y.; Miyatake, N.; Miyai, Y.; Matsumoto, K.; Wakamatsu, K.; Saito, Y.; Hara, M.; Murayama, S.; Ueno, M. Morphometry of Choroid Plexus Epithelial Cells in Neurodegenerative Diseases. *Neuropathology* **2025**, *45*, 202–209. [CrossRef] [PubMed]
19. Alisch, J.S.R.; Kiely, M.; Triebswetter, C.; Alsameen, M.H.; Gong, Z.; Khattar, N.; Egan, J.M.; Bouhrara, M. Characterization of Age-Related Differences in the Human Choroid Plexus Volume, Microstructural Integrity, and Blood Perfusion Using Multiparameter Magnetic Resonance Imaging. *Front. Aging Neurosci.* **2021**, *13*, 734992. [CrossRef] [PubMed]
20. Sun, Z.; Li, C.; Zhang, J.; Wisniewski, T.; Ge, Y. Choroid Plexus Aging: Structural and Vascular Insights from the HCP-Aging Dataset. *Fluids Barriers CNS* **2024**, *21*, 98. [CrossRef] [PubMed]
21. Li, J.; Gao, Y.; Xu, Y.; Dai, W.; Hu, Y.; Feng, X.; Wu, D.; Zhao, L.; Alzheimer's Disease Neuroimaging Initiative, and the Parkinson's Progression Markers Initiative. Morphological Changes of the Choroid Plexus in the Lateral Ventricle across the Lifespan: 5551 Subjects from Fetus to Elderly. *Neuroimage* **2025**, *318*, 121392. [CrossRef] [PubMed]
22. Novakova Martinkova, J.; Ferretti, M.T.; Ferrari, A.; Lerch, O.; Matuskova, V.; Secnik, J.; Hort, J.; for the Alzheimer's Disease Neuroimaging Initiative. Longitudinal Progression of Choroid Plexus Enlargement Is Associated with Female Sex, Cognitive Decline and ApoE E4 Homozygote Status. *Front. Psychiatry* **2023**, *14*, 1039239. [CrossRef] [PubMed]
23. Madhukar, M.; Choudhary, A.K.; Boal, D.K.; Dias, M.S.; Iantosca, M.R. Choroid Plexus: Normal Size Criteria on Neuroimaging. *Surg. Radiol. Anat.* **2012**, *34*, 887–895. [CrossRef] [PubMed]
24. Aytaç, A.; Aydın, H. Quantitative MRI Characterization of Fluid-Related Phenotypes in Pediatric Epilepsy: Deep Learning-Assisted Assessment of Enlarged Perivascular Space Burden, Regional Distribution, and Clinical Associations. *Diagnostics* **2026**, *16*, 3304. [CrossRef] [PubMed]
25. Grasso, E.A.; Bloy, L.; Kaplan, P.; Bar-Or, A.; Yeh, E.A.; Arnold, D.L.; Narayanan, S.; Marrie, R.A.; Fadda, G.; Banwell, B.L.; et al. Choroid Plexus Volume in Pediatric-Onset Multiple Sclerosis. *Neurol. Neuroimmunol. Neuroinflamm.* **2024**, *11*, e200319. [CrossRef] [PubMed]
26. Eisma, J.J.; McKnight, C.D.; Hett, K.; Elenberger, J.; Song, A.K.; Stark, A.J.; Claassen, D.O.; Donahue, M.J. Choroid Plexus Perfusion and Bulk Cerebrospinal Fluid Flow across the Adult Lifespan. *J. Cereb. Blood Flow. Metab.* **2023**, *43*, 269–280. [CrossRef] [PubMed]
27. Ozsahin, I.; Wang, X.; Zhou, L.; Xi, K.; Hojjati, S.H.; Tanzi, E.; Maloney, T.; Fung, E.K.; Dyke, J.P.; Chen, K.; et al. Divergent Neurodegeneration Associations with Choroid Plexus Volume and Degree of Calcification in Cognitively Normal APOE E4 Carriers and Non-Carriers. *Sci. Rep.* **2025**, *15*, 12818. [CrossRef] [PubMed]
28. Lee, N.; Jeong, H.; Jeong, E.; Nam, Y.; Choi, Y. Deep Learning-Based Segmentation of Choroid Plexus Calcification on Quantitative Susceptibility Mapping: A Feasibility Study. *Sci. Rep.* **2026**. [CrossRef]
29. Zhen, Z.; Zhang, R.; Gui, L.; Chen, J.; Xu, S.; Deng, L.; Yu, Y.; Liu, H.; Chen, K.; Han, Q.; et al. Choroid Plexus Cysts on 7T MRI: Relationship to Aging and Neurodegenerative Diseases. *Alzheimer's Dement.* **2025**, *21*, e14484. [CrossRef] [PubMed]
30. Tadayon, E.; Moret, B.; Sprugnoli, G.; Monti, L.; Pascual-Leone, A.; Santarnecchi, E.; for the Alzheimer's Disease Neuroimaging Initiative. Improving Choroid Plexus Segmentation in the Healthy and Diseased Brain: Relevance for Tau-PET Imaging in Dementia. *J. Alzheimer's Dis.* **2020**, *74*, 1057–1068. [CrossRef] [PubMed]
31. Incesoy, A.; Russe, M.F.; Hosp, J.A.; Wiendl, H.; Sajonz, B.E.A.; Coenen, V.A.; Urbach, H.; Reisert, M.; Demerath, T.; Rau, A. Deep Learning Informed by Contrast-Enhanced MRI Allows for Precise Segmentation of the Choroid Plexus in Non-Contrast Data. *Acad. Radiol.* **2026**, *33*, 4522–4527. [CrossRef] [PubMed]
32. Rusinek, H.; Bokacheva, L.; Chen, H.; Masurkar, A.; Osorio, R.; Betensky, R.; Vedvyas, A.; Chodosh, J.; Shao, Y.; Shepherd, T.; et al. Test-Retest Reliability of FreeSurfer Measures of Neurodegeneration. *NeuroImage* **2026**, *333*, 121920. [CrossRef] [PubMed]
33. Yazdan-Panah, A.; Schmidt-Mengin, M.; Ricigliano, V.A.G.; Soulier, T.; Stankoff, B.; Colliot, O. Automatic Segmentation of the Choroid Plexuses: Method and Validation in Controls and Patients with Multiple Sclerosis. *NeuroImage Clin.* **2023**, *38*, 103368. [CrossRef] [PubMed]
34. Zhou, L.; Butler, T.A.; Wang, X.H.; Keil, S.A.; Hojjati, S.H.; Hu, T.-W.; Savard, M.; Lussier, F.Z.; Rosa-Neto, P.; Glodzik, L.; et al. Region-Informed Machine Learning Model for Choroid Plexus Segmentation in Alzheimer's Disease. *Front. Aging Neurosci.* **2025**, *17*, 1613320. [CrossRef] [PubMed]

35. Visani, V.; Veronese, M.; Pizzini, F.B.; Colombi, A.; Natale, V.; Marjin, C.; Tamanti, A.; Schubert, J.J.; Althubaity, N.; Bedmar-Gómez, I.; et al. ASCHOPLEX: A Generalizable Approach for the Automatic Segmentation of Choroid Plexus. *Comput. Biol. Med.* **2024**, *182*, 109164. [CrossRef] [PubMed]
36. Maier-Hein, L.; Reinke, A.; Godau, P.; Tizabi, M.D.; Buettner, F.; Christodoulou, E.; Glocker, B.; Isensee, F.; Kleesiek, J.; Kozubek, M.; et al. Metrics Reloaded: Recommendations for Image Analysis Validation. *Nat. Methods* **2024**, *21*, 195–212. [CrossRef] [PubMed]
37. Storelli, L.; Pagani, E.; Rubin, M.; Margoni, M.; Filippi, M.; Rocca, M.A. A Fully Automatic Method to Segment Choroid Plexuses in Multiple Sclerosis Using Conventional MRI Sequences. *Magn. Reson. Imaging* **2024**, *59*, 1643–1652. [CrossRef] [PubMed]
38. Tohka, J. Partial Volume Effect Modeling for Segmentation and Tissue Classification of Brain Magnetic Resonance Images: A Review. *World J. Radiol.* **2014**, *6*, 855–864. [CrossRef] [PubMed]
39. Ye, S.; Lim, J.Y.; Huang, W. Statistical Considerations for Repeatability and Reproducibility of Quantitative Imaging Biomarkers. *BJR Open* **2022**, *4*, 20210083. [CrossRef] [PubMed]
40. Tahira, A.; Marques, F.; Lisboa, B.; Feltrin, A.; Barbosa, A.; De Oliveira, K.C.; De Bragança Pereira, C.A.; Leite, R.; Grinberg, L.; Suemoto, C.; et al. Are the 50's, the Transition Decade, in Choroid Plexus Aging? *GeroScience* **2021**, *43*, 225–237. [CrossRef] [PubMed]
41. Chappel-Farley, M.G.; Sewell, K.R.; Collins, A.M.; Molina-Hidalgo, C.; Jain, S.; Huang, H.; Solis-Urra, P.; Oberlin, L.E.; Grove, G.; Kramer, A.F.; et al. Greater Choroid Plexus Volume Is Linked to Poor Sleep, Neurodegeneration, and Cognitive Deficits in Older Adults: Evidence from the IGNITE Study. *Alzheimer's Dement.* **2026**, *22*, e71627. [CrossRef] [PubMed]
42. Jiang, J.; Zhuo, Z.; Wang, A.; Li, W.; Jiang, S.; Duan, Y.; Ren, Q.; Zhao, M.; Wang, L.; Yang, S.; et al. Choroid Plexus Volume as a Novel Candidate Neuroimaging Marker of the Alzheimer's Continuum. *Alzheimer's Res. Ther.* **2024**, *16*, 149. [CrossRef] [PubMed]
43. Jeong, S.H.; Park, C.J.; Cha, J.; Kim, S.-Y.; Lee, S.-K.; Kim, Y.J.; Sohn, Y.H.; Chung, S.J.; Lee, P.H. Choroid Plexus Volume, Amyloid Burden, and Cognition in the Alzheimer's Disease Continuum. *Aging Dis.* **2024**, *16*, 552–564. [CrossRef] [PubMed]
44. Pearson, M.J.; Wagstaff, R.; Williams, R.J.; for the Alzheimer's Disease Neuroimaging Initiative. Choroid Plexus Volumes and Auditory Verbal Learning Scores Are Associated with Conversion from Mild Cognitive Impairment to Alzheimer's Disease. *Brain Behav.* **2024**, *14*, e3611. [CrossRef] [PubMed]
45. Yin, F.; Wang, X.; Chen, X.; Sun, J.; Zhang, K.; Dong, X.; Wang, W.; Zeng, P.; Li, B.; Nie, L.; et al. Decoding Choroid Plexus Pathology in Alzheimer's Disease: A Longitudinal Radiomics Approach for Prodromal Identification and Risk Stratification. *CNS Neurosci. Ther.* **2026**, *32*, e70987. [CrossRef] [PubMed]
46. Hosseini, S.A.; Aumont, E.; Rahmouni, N.; Woo, M.S.; Macedo, A.C.; Hall, B.; Chan, T.; Therriault, J.; Trudel, L.; Zheng, Y.; et al. Choroidal–Ventricular System Abnormalities Are Linked to Amyloid- β Aggregation in Alzheimer's Disease. *Alzheimer's Dement.* **2026**, *22*, e71205. [CrossRef] [PubMed]
47. Xia, H.; Feng, Y.; Zhu, H.; Yang, D.; Wang, C.; Wang, Z.; Zhang, H.; Pan, W.; Zhao, Y.; for the Alzheimer's Disease Neuroimaging Initiative; et al. Association of Choroid Plexus Volume with White Matter Microstructure, Glymphatic Function, and Peripheral Systemic Inflammation in Alzheimer's Disease. *Transl. Psychiatry* **2025**, *15*, 238. [CrossRef] [PubMed]
48. Lin, W.; Chen, H.; Zhang, Z.; Zhang, Y.; Wang, X.; Guo, Y.; Qin, H.; Liu, T.; Chen, F. Multimodal MRI Reveals Impaired Glymphatic Function with Choroid Plexus Enlargement and Cerebrospinal Fluid Expansion in Alzheimer's Disease. *Sci. Rep.* **2025**, *15*, 30409. [CrossRef] [PubMed]
49. Baruch, K.; Deczkowska, A.; David, E.; Castellano, J.M.; Miller, O.; Kertser, A.; Berkutzki, T.; Barnett-Itzhaki, Z.; Bezalel, D.; Wyss-Coray, T.; et al. Aging-Induced Type I Interferon Response at the Choroid Plexus Negatively Affects Brain Function. *Science* **2014**, *346*, 89–93. [CrossRef] [PubMed]
50. Mesquita, S.D.; Ferreira, A.C.; Gao, F.; Coppola, G.; Geschwind, D.H.; Sousa, J.C.; Correia-Neves, M.; Sousa, N.; Palha, J.A.; Marques, F. The Choroid Plexus Transcriptome Reveals Changes in Type I and II Interferon Responses in a Mouse Model of Alzheimer's Disease. *Brain Behav. Immun.* **2015**, *49*, 280–292. [CrossRef] [PubMed]
51. Tijms, B.M.; Vromen, E.M.; Mjaavatten, O.; Holstege, H.; Reus, L.M.; Van Der Lee, S.; Wesenhagen, K.E.J.; Lorenzini, L.; Vermunt, L.; Venkatraghavan, V.; et al. Cerebrospinal Fluid Proteomics in Patients with Alzheimer's Disease Reveals Five Molecular Subtypes with Distinct Genetic Risk Profiles. *Nat. Aging* **2024**, *4*, 33–47. [CrossRef] [PubMed]
52. Farinas, A.; Rutledge, J.; Bot, V.A.; Western, D.; Ying, K.; Lawrence, K.A.; Oh, H.S.-H.; Yoon, S.; Ding, D.Y.; Tsai, A.P.; et al. Disruption of the Cerebrospinal Fluid–Plasma Protein Balance in Cognitive Impairment and Aging. *Nat. Med.* **2025**, *31*, 2578–2589. [CrossRef] [PubMed]
53. Levit, E.; Ren, Z.; Gonzenbach, V.; Azevedo, C.J.; Calabresi, P.A.; Cree, B.A.; Freeman, L.; Longbrake, E.E.; Oh, J.; Schindler, M.K.; et al. Choroid Plexus Volume Differentiates MS from Its Mimics. *Mult. Scler.* **2024**, *30*, 1072–1076. [CrossRef] [PubMed]
54. Wang, Q.; Lv, M.; Zhou, X.; Chen, Z.; Zhou, X.; Wu, Q.; Li, A.; He, W.; Xia, J. Association of Choroid Plexus Volume with MRI Indices of DTI-Derived Parameters and Perivascular Spaces in Patients with Neurodegenerative Diseases. *Eur. J. Radiol.* **2026**, *199*, 112798. [CrossRef] [PubMed]

55. Tejani, A.S.; Klontzas, M.E.; Gatti, A.A.; Mongan, J.T.; Moy, L.; Park, S.H.; Kahn, C.E.; for the CLAIM 2024 Update Panel; Abbara, S.; Afat, S.; et al. Checklist for Artificial Intelligence in Medical Imaging (CLAIM): 2024 Update. *Radiol. Artif. Intell.* **2024**, *6*, e240300. [CrossRef] [PubMed]
56. Marzi, C.; Giannelli, M.; Barucci, A.; Tessa, C.; Mascalchi, M.; Diciotti, S. Efficacy of MRI Data Harmonization in the Age of Machine Learning: A Multicenter Study across 36 Datasets. *Sci. Data* **2024**, *11*, 115. [CrossRef] [PubMed]
57. Hajianfar, G.; Hosseini, S.A.; Bagherieh, S.; Oveisi, M.; Shiri, I.; Zaidi, H. Impact of Harmonization on the Reproducibility of MRI Radiomic Features When Using Different Scanners, Acquisition Parameters, and Image Pre-Processing Techniques: A Phantom Study. *Med. Biol. Eng. Comput.* **2024**, *62*, 2319–2332. [CrossRef] [PubMed]
58. Puzio, T.; Matera, K.; Karwowski, J.; Piwnik, J.; Białkowski, S.; Podyma, M.; Dunikowski, K.; Siger, M.; Stasiołek, M.; Grzelak, P.; et al. Deep Learning-Based Automatic Segmentation of Brain Structures on MRI: A Test-Retest Reproducibility Analysis. *Comput. Struct. Biotechnol. J.* **2025**, *28*, 128–140. [CrossRef] [PubMed]
59. Sounderajah, V.; Guni, A.; Liu, X.; Collins, G.S.; Karthikesalingam, A.; Markar, S.R.; Golub, R.M.; Denniston, A.K.; Shetty, S.; Moher, D.; et al. The STARD-AI Reporting Guideline for Diagnostic Accuracy Studies Using Artificial Intelligence. *Nat. Med.* **2025**, *31*, 3283–3289. Correction in *Nat. Med.* **2026**, *32*, 3493. [CrossRef] [PubMed]
60. Collins, G.S.; Moons, K.G.M.; Dhiman, P.; Riley, R.D.; Beam, A.L.; Van Calster, B.; Ghassemi, M.; Liu, X.; Reitsma, J.B.; van Smeden, M.; et al. TRIPOD+AI Statement: Updated Guidance for Reporting Clinical Prediction Models That Use Regression or Machine Learning Methods. *BMJ* **2024**, *385*, e078378. Correction in *BMJ* **2024**, *385*, q902. [CrossRef] [PubMed]

Disclaimer/Publisher's Note: The statements, opinions and data contained in all publications are solely those of the individual author(s) and contributor(s) and not of MDPI and/or the editor(s). MDPI and/or the editor(s) disclaim responsibility for any injury to people or property resulting from any ideas, methods, instructions or products referred to in the content.